Thermal gradient driven enhancement of pure spin current at room temperature in nonlocal spin transport devices

S. R. Bakaul,[1,3] S. Hu,[1] and T. Kimura[1,2,*]

[1]*Advanced Electronics Research Division, INAMORI Frontier Research Center, Kyushu University, 744 Motooka, Fukuoka 819-0395, Japan*

[2]*CREST, Japan Science and Technology Agency, Sanbancho, Tokyo 102-0075, Japan*

[3]*Japan Society for the Promotion of Science, Tokyo 102-0083, Japan*

(Received 17 May 2013; revised manuscript received 25 September 2013; published 8 November 2013)

We show that the junction design in the laterally configured ferromagnetic/nonmagnetic (FM/NM) hybrid structure significantly affects the spin transport under high-bias current. The thermal conductivity mismatch between FM and NM and the inhomogeneous current distribution at the interface produce a reversed temperature gradient, which drastically reduces the thermal spin injection efficiency. The homogeneity in the temperature gradient at the interface is a crucial factor in determining the efficiency of the thermal spin current generation. The experimental results show excellent agreement with the theoretical model [Y. Takezoe *et al.*, Phys. Rev. B **82**, 094451 (2010)] that the spin relaxation is proportional to the second spatial derivative of the temperature.

DOI: 10.1103/PhysRevB.88.184407 PACS number(s): 85.80.−b, 73.50.−h, 85.75.−d

Exploiting electrons' spin degree of freedom has been sought as one of the most promising ways to meet the future need for low-power operated, ultrasmall, and multifunctional electronic devices.[1–5] The advent of laterally patterned, nonlocal spin transport devices (NSTD) is an important milestone in this regard, as these are capable of generating electronic charge-free and nondissipative pure spin current.[6–8] The most imperative and primary issue associated with these generic spintronic devices is to enhance the amplitude and generation efficiency of the pure spin current. Theoretically, the simplest way to generate large pure spin current in NSTDs is to increase the excitation charge current density, which enhances the spin splitting in the nonmagnetic (NM) spin transport channel. In practice, this technique suffers from a key bottleneck arising from the excitation current-generated Joule heat in both ferromagnetic (FM) injector and NM channels, as the spin diffusion length (λ) and the spin polarization (P) strongly deteriorate with increasing charge current, resulting in a drastic decrease of the spin generation efficiency.[9]

Although Joule heating in spin transport devices is naively considered to be disadvantageous, gradient in spatial temperature (T) causes several recently discovered spin-related phenomena, commonly dubbed as spin-caloritronic effects, such as thermal spin current,[10,11] spin-dependent Peltier effect,[12,13] spin Seebeck effect,[14] Seebeck spin tunneling,[15] and anomalous Nernst-Ettingshausen effect.[16,17] These effects can alter the pure spin current related signals, and depending on the device geometry and the flow direction of injecting charge current (I_c), both deleterious and aiding impacts are possible to achieve. Thermal spin current, in particular, is expected to relieve the Joule heat-induced obstacles in pure spin generation, although its presence is comparatively weak in typical spin transport devices.

In this work, we show that the junction design in NSTDs plays a vital role in controlling the temperature gradient landscape at the interface and thus determining the strength of thermal spin current. In certain devices, a reversed temperature gradient is generated that drastically reduces the spin current generated by the normal temperature gradient. The reversed temperature gradient is a consequence of thermal conductivity mismatch between FM and NM and inhomogeneous current distribution, which can be minimized by optimizing the junction design.

Figure 1(a) shows the scanning electron microscopy (SEM) image of the functional portion of one of the measured devices. Lateral, nonlocal spin valves with two FM injectors were fabricated on SiO_2-coated Si substrate by two-step electron beam lithography, thermal evaporation, and liftoff techniques. Permalloy (Py) and Cu were used as spin injector and transport channel materials, respectively. The two Py injectors with 100-nm width and 30-nm thickness, together with a Py detector of the same width and 10-nm thickness, were fabricated in the first two steps. The 250-nm-wide and 170-nm-thick Cu as the transport channel and the voltage measurement probes were prepared in the next step. Two types of samples were measured. In type-A samples, the injectors were placed 100 nm apart from each other, whereas type-B samples' injectors were connected to each other. To create an electronically transparent interface, prior to the Cu evaporation, a precleaning procedure on the Py layer was performed by using low-dose Ar^+ ion milling.

The pure spin current is mainly generated by a variable dc bias (I_{dc}) flowing through the injectors labeled as 1 and 2 in Fig. 1(a). A small ac probing current (peak-to-peak $dI_{ac} = 0.2$ mA) was superimposed with I_{dc}, and the amplitude of the spin current was monitored from the first harmonic voltage (dV_s) captured between the electrodes 3 and 4, by using a lock-in amplifier at room temperature. As the charge current I_{dc} flows from injectors 1 and 2 through terminal 5, pure spin is accumulated at the interface, which diffuses towards the detector FM. When the magnetic field is swept from $-(+)800$ Oe to $+(-)800$ Oe, dV_s/dI_{ac} ($= R_s$) switches from a high (low) to low (high) value, due to the parallel (antiparallel) and antiparallel (parallel) alignment between the injector and detector FM. The relative difference between the R_s in two states is termed as spin signal ΔR_s.

Figures 1(b)–1(d) show field-dependent R_s at 0, $+5$, and -5 mA dc bias, respectively, for type-A devices. For ease of comparison, the background signal has been removed from these figures. Clearly, ΔR_s is larger at negative bias than that

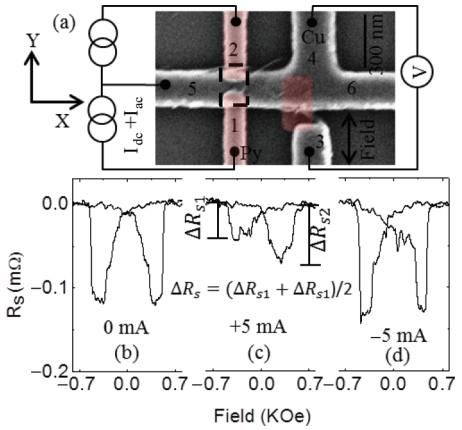

FIG. 1. (Color online) (a) Colored SEM image of the fabricated device with a gap between two Py spin injectors, and (b)–(d) show the nonlocal spin signals (dV_s/dI_{ac}) of this sample at 0, +5, and −5 mA dc bias, respectively. Due to the presence of strong thermal spin current, the spin signal is higher at negative bias and lower at positive bias than that at zero bias.

at positive bias. The bias-dependent trend of the normalized ΔR_s is plotted in Fig. 2(a), showing that unlike the positive bias branch, ΔR_s is not reduced with the increase of negative dc level, rather, it is amplified up to 11% at −5 mA, compared to that at zero bias.

Enhancement of spin signal in NSTDs at high bias has been recently reported by Wang *et al*. also.[18] It was argued that owing to the nonlinear resistivity at high-bias level, the current lines become more perpendicular to the interface; therefore, efficient spin injection becomes possible. However, this is possible only if an electrically insulating layer is present at the interface, whereas the typical resistance-area product for our Py/Cu interface is as low as 0.1 fΩ m^2.[19] Furthermore, in this case the enhancement of spin signal would be independent of the bias polarity, which is unlike our results. Thus, the possibility of the redistribution of current lines as the origin of the enhanced spin signal in our devices can be ruled out. Apart from this, in a semiconductor-based NSTD Jeon *et al*. observed a bias-dependent asymmetric spin signal and attributed it to the asymmetry in electron tunneling process.[20] However, this scenario is also inapplicable for our case as the devices are all metallic in nature.

Another phenomenon relevant to our experiments is the Peltier heating-cooling at the Py/Cu interface, which leads to a dc-bias polarity and amplitude-dependent asymmetric temperature profile at the interface. Since the spin current

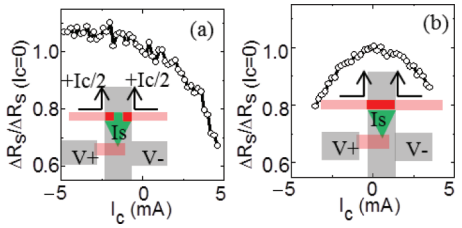

FIG. 2. (Color online) (a) Bias dependence of the normalized spin signals of (a) type-A and (b) type-B sample. The device schematics are shown in the insets.

generation efficiency depends on the temperature of the device, the Peltier effect often modifies the detected spin voltage.[21] However, according to our current flow direction notation [see the inset of Fig. 2(a)], due to Peltier heating, a negative current would increase the temperature of the interface; therefore, a reduction in spin signal is expected in this case. Therefore, the Peltier effect cannot account for the enhanced spin signal observed in our experiments.

We argue that the enhancement of spin signal at negative dc bias is a manifestation of the thermal spin injection.[10] As the resistivity of Py ($\rho_{Py} = 18\,\mu\Omega$ cm) is one order higher than that of Cu ($\rho_{Cu} = 1.7\,\mu\Omega$ cm) and the heating power is proportional to ρI_{dc}^2, Py is hotter than Cu. As a result of the generated temperature gradient (∇T) at the interface, Seebeck voltage is developed, which injects extra spin-polarized current into Cu. Since ∇T is uncorrelated to the bias current direction, at both positive and negative polarity, it provides same amount of excess up (↑) spin accumulation at the interface. On the other hand, negative and positive dc biases create ↑ and ↓ (down) spin accumulation, respectively. Therefore, total accumulated spin is enhanced at negative bias and attenuated at positive bias, causing a bias-dependent asymmetry in the detected spin signal. At low temperature, Erekhinsky *et al*. also reported asymmetric bias dependence of spin signal originating from the thermal spin current.[11] We emphasize that in our sample such thermal spin not only creates asymmetric bias dependence but also counteracts the Joule-heating-mediated degradation of spin signal at room temperature and assists the pure spin generation efficiency to transcend the value at zero dc level.

To understand the effect of removing the gap between spin injectors on the thermally generated spin current, we studied the bias-dependent response of nonlocal spin current in type-B samples [Fig. 2(b)]. Interestingly, the spin signal in this kind of devices reduces with increasing dc bias, irrespective of the current polarity. This suggests that the contribution from the thermal spin current is insignificant and the bias dependence of ΔR_s is mainly dominated by the Joule heating in this case. The slight asymmetry in it can be understood as an effect of the bias-dependent asymmetric temperature profile on the spin signal, caused by the Peltier heating (at negative dc bias) and cooling (at positive dc bias) at the interface.

Since temperature gradient generates the thermal spin current, we use the finite element program Comsol Multiphysics[22] to simulate the temperature landscape generated by the bias current $I_{dc} = 5 \times 10^{11}$ A/m^2 at the interfaces of both types of devices, which are shown in Figs. 3(a) and 3(b). The substrate is modeled as a 1-μm-thick Si coated by 300-nm-thick SiO_2 layer. The temperature at the bottom of the Si layer is fixed at 300 K. The thermal conductivities of Cu, Py, Si, and SiO_2 are 400, 46, 130, and 1.4 W m^{-1} K^{-1}, respectively. For simplicity, we do not include any thermal resistance between Cu and Py. We note that such thermal resistance affects only the magnitude of the temperature gradient, not the sign of it. An interesting feature in type-B sample's temperature landscape is that near the interface, the sign of the temperature gradients at $Y = 150$ and $Y = 300$ nm are opposite to each other, which can be noticed from the Z dependence of temperature shown in Figs. 3(c) and 3(d). This can be understood if we look at the Fourier's heat equation, which governs the temperature

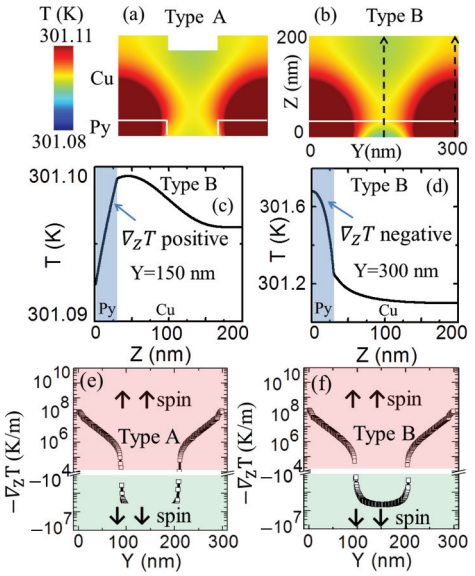

FIG. 3. (Color online) Temperature profile of the YZ plane along the center of the Py/Cu interface of (a) type-A and (b) type-B devices. The white lines define the positions of the Py electrodes. The black lines indicate places where line profiles of temperature were evaluated, and (c) and (d) show the Z dependence of the temperature of type-B sample at $Y = 150$ nm and $Y = 300$ nm, respectively. Unlike type A, type-B samples have a large Py/Cu interface area with reversed temperature gradient, which causes the minority spin injection and reduction of overall spin signal amplitude. (e) and (f) show the cross-sectional profiles of the temperature gradient along Z direction at $Z = 30$ nm of type-A and type-B samples, respectively.

profile:[23]

$$k\left(\frac{d^2T}{dx^2}+\frac{d^2T}{dy^2}+\frac{d^2T}{dz^2}\right)+\dot{g}=0. \tag{2}$$

Here, the first three terms are mainly related to the heat diffusion and governed by the thermal conductivity k, whereas the last term takes care of generated Joule heat and depends on ρ_{Py} and ρ_{Cu}. The one-order difference between ρ_{Py} and ρ_{Cu} leads to an inhomogeneous current distribution at the interface. At the edge of the interface, all the current enters through Py first and then spreads in Cu. Therefore, here the current density and generated heat are higher in Py than those in Cu, whereas the situation is reversed at the interface far from the edge. In addition, since Cu has a larger thermal conductivity than Py, heat generated in Py at the edge of the interface is more effectively transported in Cu than Py. Therefore, sign reversal of ∇T takes place at some part of the interface, especially in devices with large interface area.

Now the strong and weak presence of thermal spin currents in type-A and type-B devices can be understood as an effect of the reversed ∇T at the Py/Cu interface. The ∇T induced electric field is calculated according to the relation: $E_z = -S\nabla_Z T$ and cross-sectional profiles (at $Z = 30$ nm) are plotted in Figs. 3(e) and 3(f) respectively. Here $S = -20\ \mu$V/m is the Seebeck coefficient for Py.[24] Unlike the type-A sample, the negative electric field is generated in a large portion of the interface area of type-B sample. As a consequence, thermal spins accumulated in such area is ↓ type, which counterbalances the effect of the ↑-type thermal spin accumulated near the edge. Therefore, in this case, the overall contribution of the thermal spin injection on the detected spin signal is negligible. On the contrary, the effect of the reversed ∇T is diminished if the Py/Cu interfacial area is small, and there is a gap between the injectors, which causes strong presence of thermal spin in the detected spin signal.

The thermal spin current in a homogeneous ∇T landscape can be calculated by Eq. (1) of Ref. 10. However, in reality and as the Comsol simulation suggests, ∇T is highly inhomogeneous at the FM/NM interface of NSTD. The inhomogeneity in ∇T can increase the spin relaxation rate in FM and thus randomizes electrons' spin and reduces the effectively generated thermal spin current.[25] The theory suggests that the spin relaxation rate is proportional to the spatial double derivative of temperature ($\nabla_Z^2 T$). This is plotted in Figs. 4(a) and 4(b), showing that the spin relaxation effect is lowest at the center of the interface and highest at the edge. On the other hand, $\nabla_Z T$ is stronger at the edge than that at the center. Therefore, the magnitude of the effective thermally generated spin injection at the edge and center of the interface could be comparable. Thus, to obtain a quantitative comparison between the effective thermal spin injections at these places, $\nabla_Z^2 T$ should be included as a scaling factor in Eq. (1) of Ref. 10. Accordingly, we calculate the generated thermal spin current density in every unit cell (1 nm × 1 nm) of the interface by using the modified formula: $J_{s(Th)} = \frac{-(1-P^2)S_s}{2\rho_F}\cdot\frac{\nabla_Z T}{|\nabla_Z^2 T|}$. Taking spin polarization $P = 0.3$ and spin-dependent Seebeck coefficient $S_s = -3.8\ \mu$V/K from the literature,[10] we estimate $J_{s(Th)}$ at the interfaces of both types of devices. As shown by the cross-sectional profiles of Fig. 4(d), in type-B sample's interface both ↑ and ↓ types of spin current are present, and their magnitudes are of similar order. Summing the contributions from all unit cells, we find that the total $J_{s(Th)}$ in the type-A sample is 3.6 times larger than that in the type-B sample. This corroborates with our

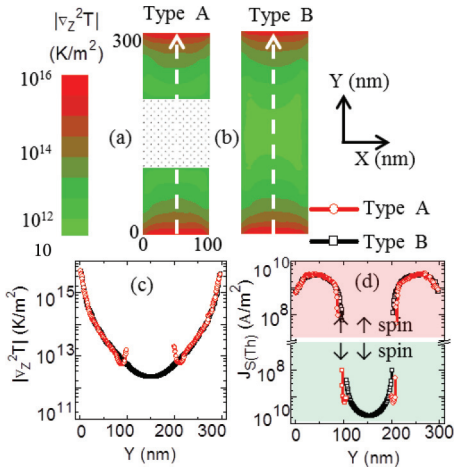

FIG. 4. (Color online) $|\nabla^2 T|$ landscape in Py under the Py/Cu interfaces of the (a) type-A and (b) type-B devices, and (c) cross-sectional profile along the dotted line of the interface area. Spin relaxation torque is large at the places where $|\nabla^2 T|$ Value is high, and (d) shows the calculated thermal spin current for both types of devices, taking spin relaxation torque into consideration.

experimental observation that the thermal spin generation is stronger in type-A samples than those in type-B samples.

To summarize, we show that in lateral NSTDs owing to the large difference between the FM and the NM's thermal conductivity and inhomogeneous current distribution in the junction, a reversed temperature gradient is developed, which reduces the generation efficiency of the thermal spin current. Such reversed temperature gradient can be diminished by creating a gap between the two spin injectors. Our results and simulation support the theoretical prediction[25] that the spatial double derivative of temperature causes spin relaxation effect, which should be considered in analyzing the thermally generated spin current and designing the structures of NSTDs.

*kimura@ifrc.kyushu-u.ac.jp

[1]G. E. W. Bauer, E. Saitoh, and B. J. Van Wees, Nat. Mater. **11**, 391 (2012).
[2]R. Jansen, Nat. Mater. **11**, 400 (2012).
[3]I. Zutic, J. Fabian, and D. S. Sarma, Rev. Mod. Phys. **76**, 323 (2004).
[4]C. Chappert, A. Fert, and F. Nguyen, Nat. Mater. **6**, 813 (2007).
[5]S. A. Wolf, D. D. Awschalom, R. A. Buhrman, J. M. Daughton, S. von Molnár, M. L. Roukes, A. Y. Chtchelkanova, and D. M. Treger, Science **294**, 1488 (2001).
[6]M. Johnson and R. H. Silsbee, Phys. Rev. Lett. **55**, 1790 (1985).
[7]F. J. Jedema, A. T. Filip, and B. J. van Wees, Nature **410**, 345 (2001).
[8]M. Johnson and R. H. Silsbee, Phys. Rev. B **37**, 5312 (1988).
[9]F. Casanova, A. Sharoni, M. Erekhinsky, and I. K. Schuller, Phys. Rev. B **79**, 184415 (2009).
[10]A. Slachter, F. L. Bakker, J.-P. Adam, and B. J. van Wees, Nat. Phys. **6**, 879 (2010).
[11]M. Erekhinsky, F. Casanova, I. Schuller, and A. Sharoni, Appl. Phys. Lett. **100**, 212401 (2012).
[12]J. Flipse, F. L. Bakker, A. Slachter, F. K. Dejene, and B. J. van Wees, Nat. Nanotechnol. **7**, 166 (2012).
[13]F. L. Bakker, A. Slachter, J.-P. Adam, and B. J. van Wees, Phys. Rev. Lett. **105**, 136601 (2010).
[14]K. Uchida, S. Takahashi, K. Harii, J. Ieda, W. Koshibae, K. Ando, S. Maekawa, and E. Saitoh, Nature (London) **455**, 778 (2008).
[15]J.-C. Breton, S. Sharma, H. Saito, S. Yuasa, and R. Jansen, Nature (London) **475**, 82 (2011).
[16]T. Miyasato, N. Abe, T. Fujii, A. Asamitsu, S. Onoda, Y. Onose, N. Nagaosa, and Y. Tokura, Phys. Rev. Lett. **99**, 086602 (2007).
[17]S. Y. Huang, W. G. Wang, S. F. Lee, J. Kwo, and C. L. Chien, Phys. Rev. Lett. **107**, 216604 (2011).
[18]X. J. Wang, H. Zou, and Y. Ji, Phys. Rev. B **81**, 104409 (2010).
[19]T. Kimura, N. Hashimoto, S. Yamada, M. Miyao, and K. Hamaya, NPG Asia Mater, **4**, e9 (2012).
[20]K. Jeon, B. Min, Y. Jo, H. Lee, I. Shin, C. Park, S. Park, and S. Shin, Phys. Rev. B **84**, 165315 (2011).
[21]S. Hu and T. Kimura, Phys. Rev. B **87**, 014424 (2013).
[22]http://www.comsol.com.
[23]Y. A. Cengel, *Heat Transfer: A Practical Approach*, 2nd ed. (McGraw-Hill, New York, 2003).
[24]A. Slachter, F. L. Bakker, and B. J. van Wees, Phys. Rev. B **84**, 020412(R) (2011).
[25]Y. Takezoe, K. Hosono, A. Takeuchi, and G. Tatara, Phys. Rev. B **82**, 094451 (2010).